


Article

Bivariate Modelling of a Teleconnection Index and Extreme Rainfall in a Small North Atlantic Island

Luis Angel Espinosa ^{1,*}, Maria Manuela Portela ¹, João Dehon Pontes Filho ² and Martina Zelenakova ³

¹ Instituto Superior Técnico (IST), Civil Engineering Research and Innovation for Sustainability (CERIS), 1049-001 Lisbon, Portugal; maria.manuela.portela@ist.utl.pt

² Hydraulic and Environmental Engineering Department (DEHA), Federal University of Ceará, Fortaleza 60020-180, Brazil; dehon@alu.ufc.br

³ Department of Environmental Engineering, Technical University of Kosice, 042 00 Kosice, Slovakia; martina.zelenakova@tuke.sk

* Correspondence: luis.espinosa@tecnico.ulisboa.pt

† Current address: Department of Civil Engineering, Architecture and Georesources (DECivil), Instituto Superior Técnico (IST), Universidade de Lisboa, Av. Rovisco Pais, No. 1, 1040-001 Lisbon, Portugal.

Abstract: This paper explores practical applications of bivariate modelling via copulas of two likely dependent random variables, i.e., of the North Atlantic Oscillation (NAO) coupled with extreme rainfall on the small island of Madeira, Portugal. Madeira, due to its small size (~740 km²), very pronounced mountain landscape, and location in the North Atlantic, experiences a wide range of rainfall regimes, or microclimates, which hamper the analyses of extreme rainfall. Previous studies showed that the influence of the North Atlantic Oscillation (NAO) on extreme rainfall is at its largest in the North Atlantic sector, with the likelihood of increased rainfall events from December through February, particularly during negative NAO phases. Thus, a copula-based approach was adopted for teleconnection, aiming at assigning return periods of daily values of an NAO index (NAOI) coupled with extreme daily rainfalls—for the period from December 1967 to February 2017—at six representative rain gauges of the island. The results show that (i) bivariate copulas describing the dependence characteristics of the underlying joint distributions may provide useful analytical expressions of the return periods of the coupled previous NAOI and extreme rainfall and (ii) that recent years show signs of increasing climate variability with more anomalous daily negative NAOI along with higher extreme rainfall events. These findings highlight the importance of multivariate modelling for teleconnections of prominent patterns of climate variability, such as the NAO, to extreme rainfall in North Atlantic regions, especially in small islands that are highly vulnerable to the effects of abrupt climate variability.

Keywords: North Atlantic Oscillation; winter extreme rainfall; Madeira Island; copulas; teleconnection; climate variability



Citation: Espinosa, L.A.; Portela, M.M.; Pontes Filho, J.D.; Zelenakov, M. Bivariate Modelling of a Teleconnection Index and Extreme Rainfall in a Small North Atlantic Island. *Climate* **2021**, *9*, 86. <https://doi.org/10.3390/cli9050086>

Academic Editor: Salvatore Magazù

Received: 13 April 2021

Accepted: 15 May 2021

Published: 19 May 2021

Publisher's Note: MDPI stays neutral with regard to jurisdictional claims in published maps and institutional affiliations.



Copyright: © 2021 by the authors. Licensee MDPI, Basel, Switzerland. This article is an open access article distributed under the terms and conditions of the Creative Commons Attribution (CC BY) license (<https://creativecommons.org/licenses/by/4.0/>).

1. Introduction

Climate tends to change at a slow pace; however, this does not mean that climate is not prone to experiencing short-term fluctuations or anomalies at seasonal or longer timescales [1,2]. For instance, with rainfall being an essential meteorological variable subject to climate system components (e.g., to the atmosphere), it can fluctuate around the average without causing the long-term rainfall average itself to change [3]. This phenomenon is a clear example of climate variability, which refers to variations in the mean state and in other statistics on spatio-temporal scales [4]—such as extreme hydrological events withdrawing too far away from long-term values. These variations result from atmospheric and oceanic circulation, which in turn is caused mostly by differential heating of the sun on Earth. Globally, atmosphere–ocean circulations may cause extreme rainfall events or even exacerbate local and regional rainfalls from season to season or year to year time periods [5,6].

Furthermore, it is acknowledged that a higher global surface temperature (GTS) increases the intensity of extreme rainfall events more greatly than that of average rainfalls [7–10]. For the North Atlantic sector, a substantial portion of the GTS variability is associated with the North Atlantic Oscillation (NAO), a hemispheric meridional oscillation with one centre of action over the subtropical Atlantic and the other near Iceland. The NAO refers to large-scale changes in atmospheric pressure at sea level (SLP), and thus, changes in GTS and rainfall [11]. The NAO-related impacts on climate, particularly in winter, extend from eastern North America to Greenland and from northwestern Africa over Europe [12]. Despite this large-scale circulation pattern being non-linear in how it reacts, it has been shown that it has largely influenced the occurrence of extreme rainfalls during its negative and positive phases, leading to stronger climate responses depending on the location in the North Atlantic or the proximity to the Atlantic Ocean (e.g., [13–15]). For instance, when the NAO is in its negative phase, pressure anomalies are not so noticeable, producing stronger-than-average easterlies. Throughout the same negative NAO phase, warmer and wetter conditions characterise the northwestern Atlantic and southern European regions, whereas colder and drier than average conditions are seen in Northern Europe [16]. Contrasting patterns occur during the NAO positive phases with generalised opposite conditions.

A remarkable feature of the NAO is the upward seasonal and annual trend shown since the late 1980s, with high positive records [17]. However, this period has also been characterised by persistent negative NAO index (NAOI) values that seem to be unprecedented in the daily observational record [18]. Some of these persistent negative anomalies have occurred since the 2009/2010 winter. In this period, the NAO swung into an extreme negative phase, escaping the long-term upward trend, fostering unusually wet conditions and apparently promoting extreme rainfall events in some North Atlantic regions, most notably in the European Macaronesia—e.g., in the Canary Islands and the Madeira Archipelago [19]. Thus, monitoring the state of the NAO at shorter timescales (e.g., at daily scale) can improve the understanding of the climate variability with regard to rainfall extremes—as performed in this research work for a small island of the Madeira Archipelago, namely, Madeira Island—and be crucial for better short-term water resource management and planning.

Although the effects of the NAO persist for some months, the closest relationships are shown in the winter period, accounting for more than one-third of the total rainfall variance from December through February [20,21]. The formulae for the relationships between NAO and extreme rainfalls in this research work are therefore based on rainfalls above a quantile threshold occurring in those months and on previous NAOI to such events, i.e., on the occurrence of unprecedented NAOI values and extreme rainfalls with a time lag.

In this study, statistical models are developed to assess (i) how persistent NAO conditions alone can model extreme daily rainfall and (ii) if considering a multivariate approach—specifically a bivariate one between NAO and rainfall—improves the assessment of climate variability in the small Portuguese island of Madeira. This island is the appropriate setting for this analysis as it shows an overall mild climate but different microclimates due to its geographical location, sharp topography, and effect of the mountain ridge and of the North Atlantic Ocean. In the mountain region of Madeira, particularly during the winter season, heavy rainfalls have triggered flash floods, landslides and debris flows (the so-called “*aliviões*”) [22] in periods that coincide with perturbation of Earth’s energy balance. In addition, during the winter of 2009/2010, the most negative NAO records were registered for the last 160 years clearly outside of the long-term averages or trends [23] along with extreme rainfall, which in turn led to numerous hazards and casualties for the same winter period. Although rare, hydrological extreme events, such as extreme rainfall, have caused loss of life and had negative economic and social impacts on the island. Therefore, the need for appropriate statistical models of extreme hydro-meteorological events linked to large-scale atmospheric phenomena, i.e., teleconnection, becomes clear, particularly in the current context of a more recent pronounced climate variability.

Extreme rainfall events have often been linked to the strong climatic conditions and climate variability in the North Atlantic and adjacent land areas. For instance, Wilby et al. [24] investigate correlations between extreme rainfall and other climatic variables in the British Isles in relation to decadal variations in the atmospheric circulations—in terms of the NAOI—during winter. Trambly et al. [25] provide a regional assessment of trends and variability in extreme rainfall over Maghreb countries—the western and northern African countries of Morocco, Tunisia, Algeria, and Libya—showing that extreme rainfalls exhibit a strong spatial variability and are moderately correlated with large-scale atmospheric patterns such as the NAO, but also with the El Niño Southern Oscillation (ENSO), as described in [26]. Further, the NAO has also been found to affect the intensity and frequency of extreme rainfall. Queralt et al. [27] analysed 102 rain gauges with daily records over Spain and the Balearic Islands from 1997 through 2006, arguing that NAO exerts a clear effect on the increasing intensity of total and extreme rainfall rates in northern and westernmost Spanish regions and on the increasing rainfall frequency in central and southwestern areas. Specifically for Madeira Island, very few studies have been undertaken to understand the influence of the NAO on extreme rainfall. As an example, Espinosa et al. [18] focus on short-term climatic fluctuations in the NAO (e.g., daily NAOI) and claim the existence of systematic evidence of statistical dependence over Madeira between exceptionally daily negative NAOI (−NAOI) records and extreme regionalised rainfalls, based on a bivariate extremal dependence analysis, which is stronger in sustained NAOI year-long periods. It is in this context that the relevance of this study is emphasised by assessing some of the climate variability aspects.

Such an assessment was conducted with the use of copulas [28] to model the bivariate dependence between daily NAOI and extreme daily rainfall in Madeira, from 1967/1968 to 2016/2017, assuming both variables exhibit different marginal behaviours. Copulas have been recently used to determine the conditional probabilities and return periods of multivariate problems. Wong et al. [29] fitted a trivariate copula to drought characteristics, i.e., drought magnitude, duration and intensity, for some Australian rainfall districts. André and de Zea Bermudez [30] analysed and characterised the dependence using copulas between daily maximum wind speeds observed in mainland Portugal and simulate daily maximum wind speeds produced by a numerical physical model. Gouveia-Reis et al. [31] investigate the dependence of Madeira's rainfall data and spatial variables (altitude, slope orientation, distance between rain gauges, and distance to the sea) within an extreme value copula approach through an analysis of maximum annual data. To the best of the authors' knowledge, a more complex framework with at least one large-scale atmospheric pattern as a predictor—in this research work, the state of daily NAO—and extreme rainfall as a response variable has not yet been addressed.

The present paper is structured as follows. A brief description of the study area, the data used, and copula are given with a focus on bivariate return periods. The extreme winter daily rainfalls at six rain gauges in the island are first selected based on an empirical percentile as a threshold. A low-pass filter is applied to the daily NAOI series. The correlation between extreme rainfalls and previous smoothed NAOI, i.e., with a lag in between, is assessed. The bivariate observations for marginals selection and copula modelling are determined. Bivariate copula models for NAOI and extreme rainfalls are developed and compared. The selected copulas are then used to determine the bivariate joint and conditional return periods, in addition to univariate return periods, to assess the climate variability of the NAO and rainfall for Madeira Island from a multivariate perspective. The marginal and copula selection and the climate variability assessment are also discussed.

2. Physical Features of the Study Area

Madeira is the largest island of the Madeira Archipelago with an area of approximately 740 km², a length of 58 km and a 23 km width. Centred at 32°75' N and 17°00' W, the small island of Madeira—according to its size [32]—is completely shaped by volcanic materials,

consisting of an enormous east-to-west (EW) oriented mass that is cut by deep valleys [33]. Madeira has a mountain ridge that extends mainly along the central part of the island with the highest peaks in the eastern part, Pico Ruivo (1862 m.a.s.l.) and Pico do Areeiro (1818 m.a.s.l.), while the Paúl da Serra plateau (approx. 24 km² above 1400 m.a.s.l.) is located in the western part, as shown in Figure 1. The abrupt orography of peaks and valleys, together with the North Atlantic effect, provide the island with a great variety of microclimates, mostly with a mild summer and winter, except for the highlands, where the lowest temperatures are registered [34].

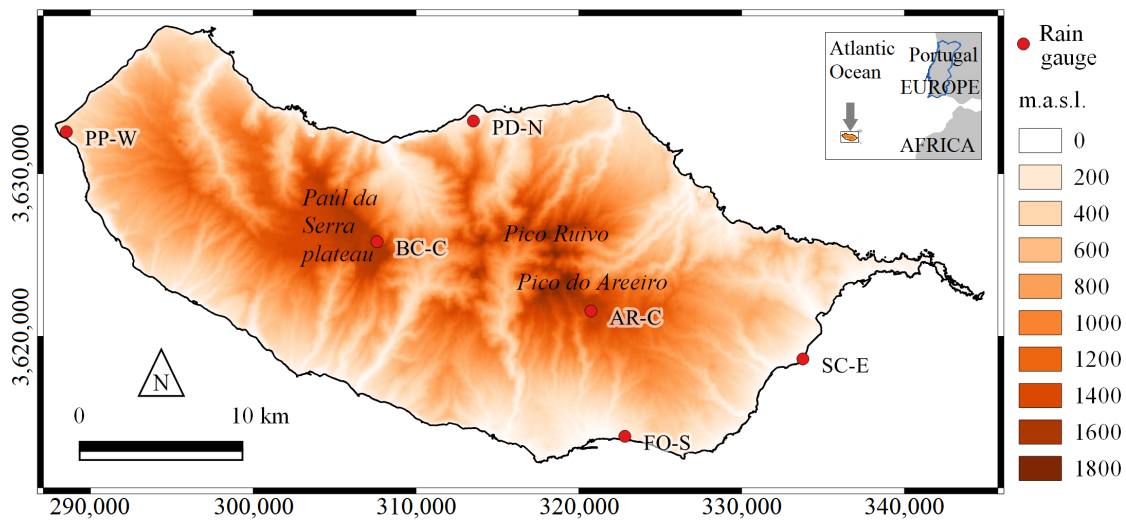


Figure 1. Coordinates WGS84 (UTM zone 28N) and relief of Madeira Island, Portugal. Spatial distribution of the six rain gauges used in this study are depicted by bullets and their identification codes (description in Table 1).

The rainfall regime over the Madeira is affected by local circulation and also by synoptic systems such as fronts and extratropical cyclones [22]. The distribution of rainfall presents an evident seasonal pattern, thoroughly different between the rainy season, that extends from November to March, and the dry season, with insignificant rainfall amounts during July and August [35]. The pronounced spatial variability of the rainfall in Madeira is determined mostly by the topography and the trade winds or easterlies—the permanent EW prevailing winds that flow in the Earth’s equatorial region [36]—with higher amounts in the northeast (~ 1600 mm year⁻¹) and central highlands (~ 2300 mm year⁻¹) than in the western (~ 800 mm year⁻¹) and southern regions (~ 600 mm year⁻¹), as previously characterised by Espinosa and Portela [37].

Table 1. The six rain gauges adopted in the study. Identification (code and name), coordinates WGS84 (UTM zone 28N), and elevation. In the code, the character after the hyphen indicates the location of the gauge, i.e., C for centre and S, N, W, and E for southern, northern, western, and eastern coastal areas, respectively.

Code	Name	UTM-X Easting (m)	UTM-Y Northing (m)	Elevation (m.a.s.l.)
AR-C	Areeiro	320,746.000	3,621,552.000	1610.0
BC-C	Bica da Cana	307,604.000	3,625,815.000	1560.0
FO-S	Funchal Observatório	322,831.000	3,613,854.000	58.0
PD-N	Ponta Delgada	313,525.801	3,633,232.797	123.0
PP-W	Ponta do Pargo	288,512.995	3,632,569.609	339.0
SC-E	Santa Catarina	333,770.000	3,618,611.000	49.0

3. Materials and Methods

To assess the climate variability from 1 December 1967 to 28 February 2017, it was vital to derive some connected schemes of relationship or teleconnections to the NAO

from extreme daily rainfall events. To this end, the rainfall daily data from December to February (DJF) of the following year were considered at six rain gauges of the island, with the expectation that different rainfall regimes would be identified due to their location: in the northern, southern, eastern and western slopes, and in the central ridge and plateau. The rainfalls above the 99th empirical percentile rank were considered as extreme rainfall events—following the recommendation of the Expert Team on Climate Change Detection, Monitoring and Indices (ETCCDMI) [38]. Based on the considered period, the number of selected rainfalls is 90 consecutive days over 50 years. Out of the 4500 days of winter DJF rainfall at each rain gauge, the highest 45 rainfalls, i.e., 1%, were chosen as extreme rainfall events.

Different smoothed NAOI series were considered—by simple averages—relating to their running length, m , and to the lag between the ending day of the smoothed series and the day of occurrence of each extreme rainfall event, l . The Pearson linear correlation [39] was applied to analyse the relationship between the smoothed and lagged values of NAOI and the selected extreme rainfalls events. Based on this correlation analysis, (i) the smoothing factor or low-pass filter [40] of m NAOI daily values and (ii) the number of lagged days, l , between the end of the smoothed NAOI values and the occurrence of extreme rainfalls were selected. This analysis was based on the rainfall data at Areiro rain gauge (AR-C in Figure 1). This rain gauge is located at the central highlands, an area that highly contributes to the island's fresh water availability and aquifer recharge due to the high rainfall and geological conditions prone to infiltration [35]. The previous NAOI values (smoothed and lagged NAOI) based on the preceding correlation analysis were assigned to the extreme rainfalls. The m and l achieved based on AR-C were applied to the other five stations so that the final dataset for copulas modelling could be assembled.

Subsequently, the Wald–Wolfowitz runs test [41] was used to test the null hypothesis H_0 of independence for the observations of the final dataset (either NAOI values or extreme rainfalls). The second part of the methodology consisted of the bivariate analysis of NAOI as the “cause” of extreme rainfall using copulas by modelling such teleconnection. Finally, the concept of bivariate return period was applied for the events defined by the joint behaviour of pairs of the random variables adopted, i.e., daily NAOI and extreme daily rainfall. This was the core of the climate variability assessment for the island of Madeira.

3.1. Rain Gauge Data

The daily rainfall data at six representative rain gauges located at the central highlands (AR-C and BC-C), southern (FO-S), northern (PD-N), western (PP-W), and eastern (SC-E) slopes, were used—Table 1 and Figure 1. The data for the time-frame from December 1967 to February 2017 were made available by IPMA—Portuguese Institute for the Ocean and Atmosphere (<https://www.ipma.pt/en/>, accessed on 20 January 2018). The data had some gaps that were filled, as described by Espinosa et al. [42]. IPMA is the national authority in the fields of meteorology, aeronautical meteorology, climate, seismology, and geomagnetism, and an institution of reference at the international level also devoted to the promotion and coordination of scientific research. For each of the rain gauges, 4500 winter daily rainfall data were retrieved, i.e., 90 DJF daily values for 50 years (excluding leap year days).

3.2. North Atlantic Oscillation Index (NAOI) Data

The large-scale atmospheric characteristics were identified through the analysis of a synoptic meteorological index for the North Atlantic Oscillation, i.e., NAOI, at the daily scale, retrieved from the portal of the NOAA Physical Sciences Laboratory, NOAA PSL [43]. The NAOI represents a pattern of low-frequency tropospheric height variability. This measure of pressure difference is based on centres of action of 500 millibars constant pressure (mb) height patterns. Note that these height fields are spectrally truncated to total wave number 10 in order to emphasise large-scale aspects of teleconnection. The calculation of this teleconnection index utilises the ESRL/PSD Global Ensemble Forecasting System

Reforecast2 (GEFS/R) ensemble forecasts from the averaged region 55–70° N; 70–10° W, which in turn is subtracted from 35–45° N; 70–10° W. The NAOI daily records were utilised for the same period as in the case of daily rainfall (DJF, from 1967/1968 through 2016/2017), but also include the months of September, October, and November, prior to each December.

3.3. Bivariate Copula

The problem of specifying a probability model for dependent bivariate observations can be greatly simplified by expressing the corresponding joint distribution F_{XY} in terms of its marginals, F_X and F_Y , and an associated dependence function copula C —introduced by Sklar [44]—completely defined through the functional identity $F_{XY} = C(F_X, F_Y)$. C is a bivariate copula, hereafter copula. It is precisely the copula that captures the features of a joint distribution. Moreover, copulas measure the association and dependence structure properties connecting random variables. In this research work, a possible way of analysing bivariate data (NAOI, X , and extreme rainfall, Y) consisted of investigating the dependence function and the marginals separately. This approach was convenient for the climate variability assessment, as this allowed studying the dependence structure independently of any marginal effect. Regardless of the marginal laws involved, the analysis of this research work was focused on practical applications of modelling copulas for teleconnection and not on the equations involved. Nevertheless, the main mathematical descriptions related to the copula concept [44] are presented next.

Definition 1. Let $\mathbb{I} = [0, 1]$; a copula is a bivariate function $C : \mathbb{I} \times \mathbb{I} \rightarrow \mathbb{I}$ such that (1) uniform marginals: for $u, v \in \mathbb{I}$, it holds that $C(u, 0) = 0, C(u, 1) = u, C(0, v) = 0$, and $C(1, v) = v$; and (2) two-increasing: for $u_1, u_2, v_1, v_2 \in \mathbb{I}$, such that $u_1 \leq u_2$ and $v_1 \leq v_2$, it holds that $C(u_2, v_2) - C(u_2, v_1) - C(u_1, v_2) + C(u_1, v_1) \geq 0$; where C is uniformly continuous on \mathbb{I}^2 . Hereafter F_X, F_Y (respectively, F_U, F_V) will denote the marginal distribution functions of the random variables X, Y (respectively, U, V).

Theorem 1. (Sklar). Let F_{XY} be a joint distribution function with marginals F_X and F_Y . Then, there exists a copula C such that

$$F_{XY}(x, y) = C(F_X(x), F_Y(y)) \tag{1}$$

for all real x, y . If F_X, F_Y are continuous, then C is unique; otherwise, C is uniquely defined on $\text{Range}(F_X) \times \text{Range}(F_Y)$. Conversely, if C is a copula and F_X, F_Y are distribution functions, then F_{XY} , given by Equation (1), is a joint distribution function with marginals F_X and F_Y . The detailed proof of Sklar’s Theorem can be found in the work of Schweizer and Sklar [45].

In addition, since $C_{X,Y}$ is invariant under strictly increasing transformation of X and Y , by virtue of the Probability Integral Transform, the pair of random variables can be expressed as (U, V) , where

$$\begin{cases} U = F_X(X) \\ V = F_Y(Y), \end{cases} \tag{2}$$

with $(U, V) \sim C_{U,V} = C_{X,Y}$. With U and V being non-exceedance probabilities given by the marginal distribution functions, they are uniform on \mathbb{I} , i.e., $U \sim \mathcal{U}(0, 1)$ and $V \sim \mathcal{U}(0, 1)$ ref. [46]. Hereafter, (X, Y) is considered as the pair of NAOI and extreme rainfall variables—and also the pair (U, V) , respectively—having a direct practical meaning.

Given a bivariate distribution function F with invertible margins F_X and F_Y , a bivariate copula $C(u, v)$ for $u, v \in [0, 1]$ is given by Equation (3). Meta-elliptic copulas are symmetric and hence lower and upper tail dependence coefficients are the same.

$$C(u, v) = F(F_X^{-1}(u), F_Y^{-1}(v)) \tag{3}$$

The Archimedean copulas are more flexible than Meta-elliptic and can present lower or upper tail dependences, which are defined by Equation (4):

$$C(u, v) = \varphi(\varphi^{-1}(u) + \varphi^{-1}(v)) \tag{4}$$

where φ is the generator function of the copula C and $\varphi[0, 1] \rightarrow [0, \infty]$ is a continuous and factually reducing function. The Meta-elliptic Gaussian and Student's t , and the Archimedean Clayton, Frank, and Gumbel, were tested to verify best fit. Table 2 presents the formulations of the candidate copula families. When the Archimedean copula is rotated 180°, it is called a survival copula and can invert the predefined tail dependence to best fit the data.

Table 2. Copula candidate family and mathematical formulation.

Copula Class	Copula Family	Mathematical Formulation
Meta-elliptic	Gaussian	$\phi_\rho(\phi^{-1}(u), \phi^{-1}(v))$
	Student's t	$T_{\rho, \nu}(T_\nu^{-1}(u), T_\nu^{-1}(v))$
Archimedean	Clayton	$(u^{-\theta} + v^{-\theta} - 1)^{-\frac{1}{\theta}}$
	Frank	$-\theta^{-1} \log \left[1 + \frac{(e^{\theta u} - 1)(e^{\theta v} - 1)}{(e^\theta - 1)} \right]$
	Gumbel	$\exp \{ - [(-\ln u)^{-\theta} + (-\ln v)^{-\theta}]^{\frac{1}{\theta}} \}$

3.3.1. Copula Parameter Estimation

The parameters for the candidate copula families were estimated considering the maximum likelihood MLE method, by choosing the Inference Functions from the Margins (IFM) method [47]. The use of the IFM method requires previous fitting of marginal distribution functions to transform the variables' values into the (0, 1) interval.

3.3.2. Best-Fitted Copula

To compare the bivariate copula models from a number of families and choose the best-fitted model, the fit statistic AIC was used. First, all the candidate copulas, Gaussian, Student's t , Clayton, Frank, and Gumbel, were fitted using a maximum likelihood estimation, MLE. Then the AIC was computed for all copula families and the one with the minimum AIC was chosen. According to Brechmann and Schepsmeier [48], for observations u_j and v_j with $j = 1, \dots, N$, the AIC of a bivariate copula family C with θ parameter(s) is defined by Equation (5):

$$AIC = -2 \sum_{i=1}^N \ln[C(u_j, v_j | \theta)] + 2k \tag{5}$$

where one parameter's copulas has $k = 1$ and the two-parameter Student's t has $k = 2$. The two-parameter copula was penalised in the minimisation of the AIC value to reduce possibility of overfitting due to the parsimony principle.

3.3.3. Bivariate Return Periods

In this subsection, the concept of a return period for events defined by their joint behaviour of pairs of random variables is introduced. This concept was applied to emphasise the particular facets of the dynamics of the considered NAOI—with particular emphasis on the negative phase of the NAO—and extreme rainfall phenomenon in Madeira Island. However, first, some necessary concepts are mathematically described as follows.

Among the several definitions of the return period, Shiau and Shen [49] describe it as the average elapsed time between occurrences of the event with a certain magnitude or greater than a threshold. The higher the return period, the more exceptional the event

is. The univariate return periods of NAOI and extreme rainfall, based on the concept of stochastic processes, are derived as follows. The return period, adapted from [49–51], of the NAOI (T_{NI}) or extreme rainfall (T_{RN}), is expressed as function of the expected interarrival time $E(L)$ and of the cumulative distribution functions (CDFs) of the NAOI, $F_{NI}(ni)$, and the extreme rainfalls, $F_{RN}(rn)$, as defined in Equations (6) and (7), respectively (marginal distributions). Note that, in this case, T and $E(L)$ are expressed in years. The $E(L)$ was obtained by dividing the 45 bivariate events (based on the chosen extreme rainfalls) by the 50 analysed years, resulting in 0.9 year for each of the six rain gauges.

$$T_{NI} = \frac{E(L)}{P(NI \geq ni)} = \frac{E(L)}{1 - F_{NI}(ni)} \quad (6)$$

$$T_{RN} = \frac{E(L)}{P(RN \geq rn)} = \frac{E(L)}{1 - F_{RN}(rn)} \quad (7)$$

Assuming that the phenomenon studied here has a multivariate nature, the return periods of the bivariate distributed NAOI and extreme rainfall events were computed as joint and conditional return periods based on the works by Shiau [52], but for drought analysis from a multivariate perspective in this case. Thus, the joint NAOI and extreme rainfall return period can be defined for $NI \geq ni$ and $RN \geq rn$, as described in Equation (8):

$$T_{NI \& RN} = \frac{E(L)}{P(NI \geq ni, RN \geq rn)} = \frac{E(L)}{1 - F_{NI}(ni) - F_{RN}(rn) + C(F_{NI}(ni), F_{RN}(rn))} \quad (8)$$

where $T_{NI \& RN}$ is the return period for $NI \geq ni$ (NAOI) and $RN \geq rn$ (extreme rainfall).

Analogously, the conditional return period was calculated for the case when NAOI is the cause of extreme rainfall, i.e., the return period of extreme rainfall given that the previous NAOI is lower than a certain threshold ($T_{RN|NI \geq ni}$). This conditional return period is calculated by Equation (9):

$$T_{RN|NI \geq ni} = \frac{T_{NI}}{P(RN \geq rn, NI \geq ni)} = \frac{E(L)}{[1 - F_{NI}(ni)][1 - F_{NI}(ni) - F_{RN}(rn) + C(F_{NI}(ni), F_{RN}(rn))]} \quad (9)$$

Further discussion on the calculations and relationships between univariate, bivariate, and conditional return periods is out of the scope of this paper. However, this can be found in the work of Shiau [52].

4. Results

The results are structured as follows. In Section 4.1, the characteristics and temporal distribution of the 45 winter extreme daily rainfalls, from 1 December to 28 February of the following year (DJF), during the considered 50 years (1967/1968–2016/2017), are shown at each of the six adopted rain gauges in Madeira Island. Then, in Section 4.2, the correlations between both the non-smoothed ($m = 0$) and smoothed daily NAOI series (after applying a low-pass filter $m \geq 0$) and extreme daily rainfall events at AR-C (Areeiro rain gauge) are presented under the assumption that the NAO is the major stressor of extreme rainfall. Different running lengths, m , and time lags, l , were tested for the NAOI, aiming at identifying the coupled series of previous NAOI and extreme rainfalls with maximum correlation. The m and l based on AR-C were then applied to the other five rain gauges, thus making up the final dataset with 45 bivariate observations at the six rain gauges in total. Subsequently, the overall strength of the association between previous NAOI and extreme rainfalls is described. In Section 4.3, the estimation of the bivariate joint distributions along with the copulas' construction are shown. Finally, in Section 4.4, the results of the bivariate return periods based on the chosen copulas for the NAO and extreme rainfall phenomena are presented.

4.1. Extreme Daily Rainfall Distribution Analysis

The analysis of the winter (DJF) extreme daily rainfalls from 1967/1968 through 2016/2017 at the representative rain gauges indicates a particularly differentiated distribution of extreme events over Madeira. The highest daily rainfall values (≥ 200 mm) were systematically recorded at the island's central highlands and plateau, i.e., at the AR-C (Areeiro) and BC-C (Bica da Cana) rain gauges (Figure 2a). The lowest extreme daily rainfalls (≤ 50 mm) occur in the coastal southern, eastern, and western areas (approximately 60.0 m.a.s.l.), namely, at FO-S (Funchal Observatório), SC-E (Santa Catarina), and PP-W (Ponta do Pargo). The remaining rain gauge, i.e., PD-N (Ponta Delgada) in the northern slope displays a mixed distribution (50–150 mm). Furthermore, Figure 2a shows a concentration of highly extreme rainfalls from all the six rain gauges—including their corresponding maximum historic records in most cases—during the years 2010 and 2011. From the same figure, the comparison between the maximum values and the lowest ones suggests that the sharp topography of the island has a major role in the extreme rainfall distribution. However, when making the extreme rainfalls dimensionless, by dividing by the corresponding averages, as represented in Figure 2b, the different series show similar behaviours, i.e., a similar temporal variability around the average, with the most extreme occurrences also concentrated in the winter of 2009/2010 and 2010/2011.

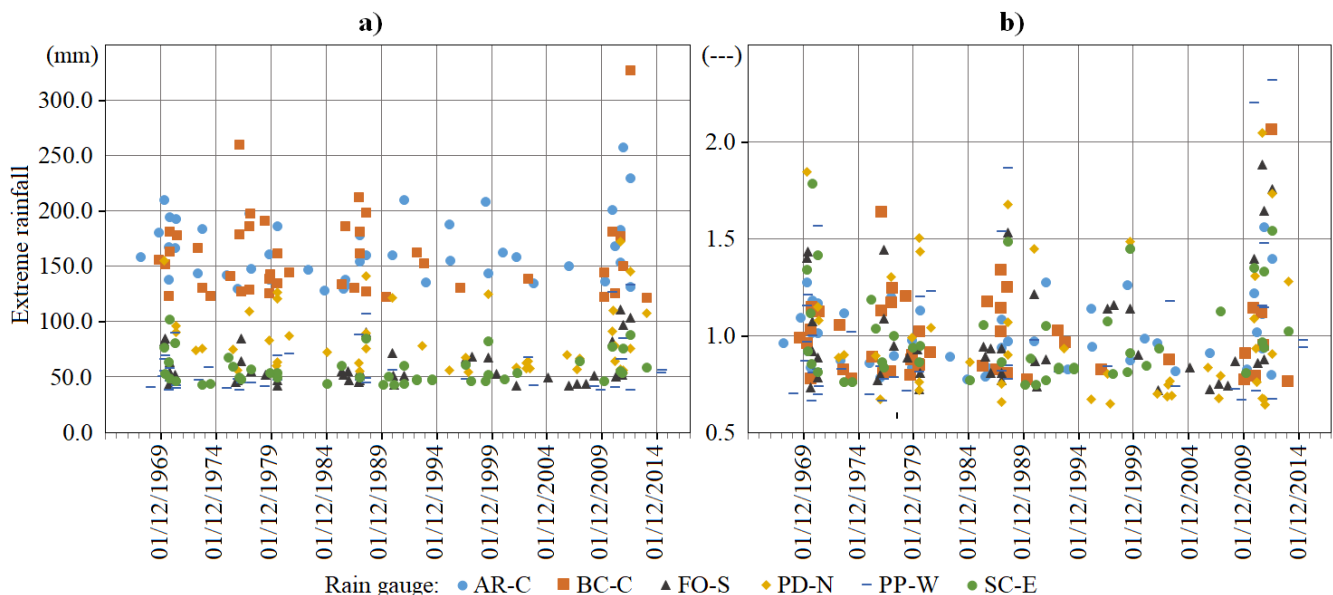


Figure 2. The winter (DJF) extreme daily rainfalls, i.e., the highest 45 rainfalls or 1% of the retrieved 4500 daily data at each rain gauge from 1967/1968 through 2016/2017, in absolute (a) and dimensionless (b) terms.

4.2. Alignment of the NAOI and Extreme Rainfall Series

The analysis between (i) smoothed and lagged NAOI values and (ii) extreme rainfall events was inspired by the extreme rainfall event of 20 February 2010 that triggered deadly debris flow occurrences in Madeira [22]. The daily rainfall records of that event were assigned to 9:00 am of the next day. A preliminary analysis of the NAOI suggested that such event could be teleconnected to the persistence of strongly negative values in previous days. Figure 3 exemplifies an extract of the non-smoothed (1d) and smoothed NAOI values—from 2 days (2d) to 30 days (30d), i.e., low-pass filter m from 2 to 30, respectively—from December 2009 to February 2010. In the figure, consecutive negative NAOI values can be observed in the first days of January 2010.

As mentioned, the effect of smoothed previous NAOI values on extreme rainfall events was assessed for the candidate rain gauge of Areeiro (AR-C), aiming at developing a criterion to align the bivariate series, which was then applied to the other rain gauges. AR-C has almost complete historic daily data and some of the island's heaviest rainfall

records, such as those that triggered the “*aluviões*” (debris flows) on 20 February 2010. This assessment ascertained an alignment or cause–effect between the X (smoothed and lagged NAOI) and Y (extreme rainfall) series by maximising the Pearson correlation applied to the 45 selected extreme rainfall events at AR-C (depicted in Figure 2a). This made it possible to identify (i) the running length, m , of the low-pass filter of daily NAOI records, and (ii) the lag in days, l , between the end of the smoothed NAOI series and the extreme rainfalls that occurred after that end.

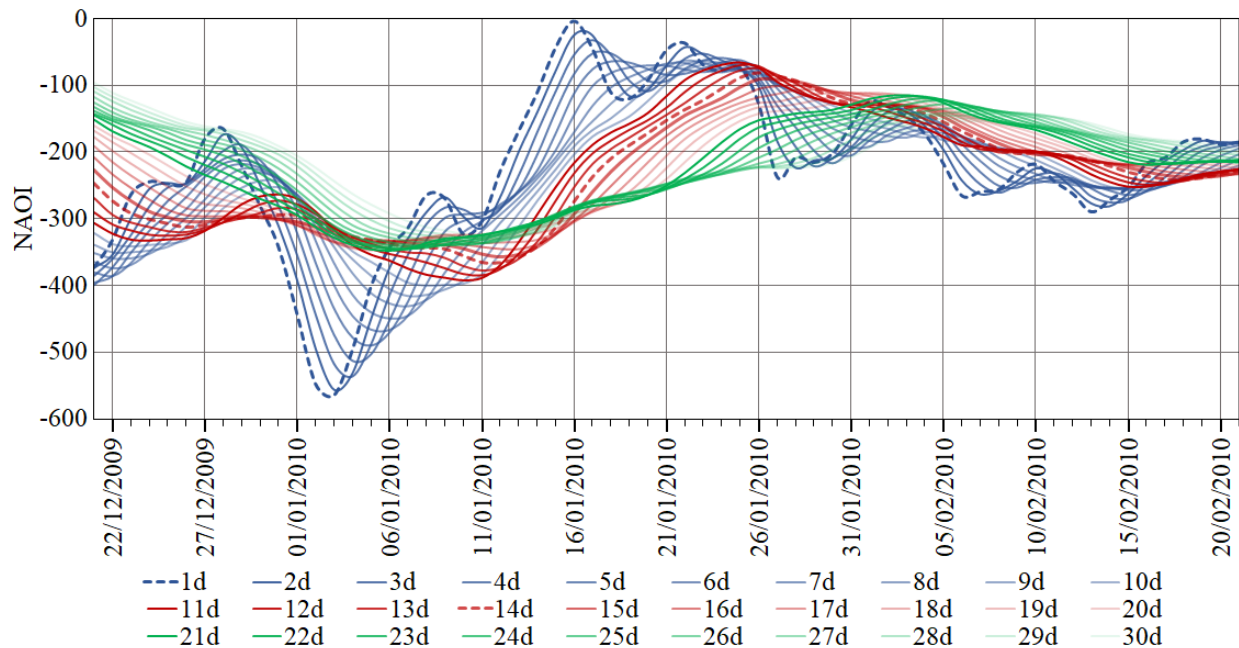


Figure 3. Example of the non-smoothed (1d) and smoothed daily NAOI series in a period prior to the 20 February 2010 flash floods, landslides and debris. The smoothed NAOI values were computed by a low-pass filter, or moving average, from the previous 2 days (2d, $m = 2$) to previous 30 days (30d, $m = 30$) and assigned to the most recent record date.

As a result of the previous analysis, a maximum value of $r = -0.84$ for the Pearson correlation coefficient was obtained based on the low-pass filter of $m = 14$ (14d) averaged NAOI values, ending 39 days prior to the extreme rainfalls events—depicted in Figure 4. For m values lower and higher than 14, but also for l values shorter and longer than 39 days, the correlations between coupled NAOI values and extreme rainfalls yielded no statistically significant improvements.

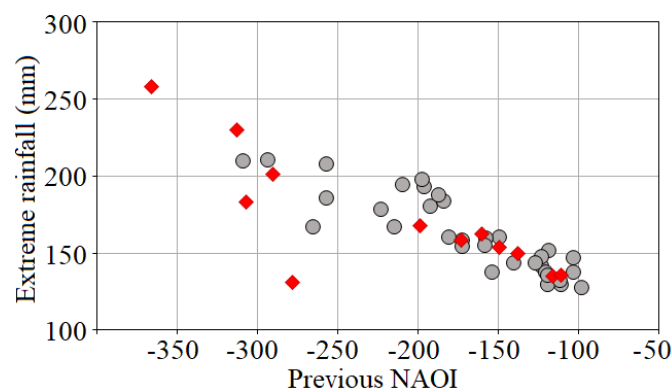


Figure 4. Scatter plot of previous smoothed NAOI and extreme rainfalls, both at daily scale, for $m = 14$ and $l = 39$ days. The 45 bivariate observations (1967/1968–2016/2017) at the AR-C rain gauge are depicted by bullets and red diamonds, the latter being the events that occurred between December 2000 and the end of the reference period. The correlation (r) between previous NAOI and extreme rainfalls is -0.84 .

In order to establish the final dataset for teleconnection via copulas, the same $m = 14$ and $l = 39$ days for NAOI—hereafter referred to as previous NAOI values—were adopted at the other rain gauges, rather than repeating the analysis for each of them. The main purpose of this was to conclude on to what extent the results obtained based on AR-C could be adopted over the island, thus simplifying further analysis on the effect of the NAO persistence over the rainfall regime in Madeira. Albeit based on the same m and l , the previous NAOI values assigned to the extreme rainfalls may differ among rain gauges due to the different dates of occurrence of those events.

The copulas modelled in this research work corresponded to *all the variables being independent* [53]. This is the copula type of any random vector established by independent variables. The elements of the extreme rainfall series may, in practice, be assumed to be independent [41]. In some cases, however, there may be significant dependence among extreme values even though they are random in a series. Conversely, independence implies that no observation in the data series has any influence on any following observations. In this regard, the independence of the univariate vectors of previous NAOI and extreme rainfalls was evaluated via the Wald–Wolfowitz runs test having the null hypothesis H_0 of independence with 0.05 as the critical value. The null hypothesis was tested at the six stations, resulting in p -values ranging from 0.31 to 0.97, for previous NAOI, and from 0.11 to 0.79, for extreme rainfall. As these results are greater than the critical value, it was not possible to reject the H_0 of independence in any case.

4.3. Bivariate Joint Distributions and Constructed Copulas

Before showing the dependence modelling of the two random variables via copulas, the resulting descriptive statistics of the bivariate series are presented in Table 3. As the values of the previous NAOI are always negative, in the copulas models, NI refers to their opposites. Additionally, given that the number of extreme rainfalls events and of analysed years are the same for the six rain gauges, the resulting $E(L)$ is also the same (0.90). The Kendall's τ correlation coefficient presents a high negative value for AR-C, which is in accordance with the visible dependence in the scatter plot set out in Figure 4, and with the Pearson correlation (r). Still, Kendall's τ measures only the overall strength of the association between previous NAOI and extreme rainfall, but does not provide accurate information about how this association varies across the distribution [54]. The mean values of extreme rainfall suggest similar characteristics at the central highlands (AR-C and BC-C), with higher values than the lowlands (e.g., FO-S and PP-W), as previously identified (Section 4.1). Concerning the mean of previous NAOI, values are homogeneous in the six series. Note that the most negative previous NAOI (min of -366.03) always appears in the coupled series. Such a value resulted from consecutive strongly negative NAOI in the first days of January 2010 (Figure 3) that was assigned to the rainfalls on 20 February 2010. The previous assessment is somewhat unclear since it is based on a univariate perspective that justifies a copula-based characterisation of the bivariate dependency structure.

Table 3. Statistics of the bivariate observations (previous NAOI and extreme rainfall) at each rain gauge from 1967/1968–2016/2017. $E(L)$ is the expected interarrival time, and Kendall tau (τ) correlates the two variables.

Rain Gauge	Number of Observations	$E(L)$ (year)	Kendall tau (τ)	Previous NAOI, $-NI$				Extreme Rainfall (mm), RN			
				Mean	Min	SD	CV	Mean	Max	SD	CV
AR-C	45	0.90	−0.71	−183.31	−366.03	69.42	−0.38	165.00	257.60	29.64	0.18
BC-C	45	0.90	−0.51	−185.08	−366.03	58.52	−0.32	159.03	327.30	39.19	0.25
FO-S	45	0.90	−0.50	−174.85	−366.03	78.25	−0.45	58.94	111.00	17.65	0.30
PD-N	45	0.90	−0.29	−177.44	−366.03	70.70	−0.40	84.03	172.10	30.37	0.36
PP-W	45	0.90	−0.27	−173.34	−366.03	80.92	−0.47	57.53	133.30	22.20	0.39
SC-E	45	0.90	−0.42	−180.94	−366.03	72.98	−0.40	57.16	101.90	14.21	0.25

The bivariate joint distributions between previous NAOI and extreme rainfall were determined to model copulas for teleconnection, aiming at obtaining the corresponding return periods. One copula function was selected for each rain gauge, as indicated in Section 3.3. Table 4 reports the selected copulas for the bivariate series based on the marginal distributions of previous NAOI and extreme rainfall. The estimated parameters and values of the goodness-of-fit test (AIC) for the best-fitted copulas and marginal distributions are listed in the same table. The selection of marginals for the individual variables (log-normal in most cases) allowed us to model the dependence structure via copulas. Only AR-C and SC-E have the same selected copula family, i.e., Survival Gumbel, whether different copulas were assigned to the other four rain gauges. This means that the joint bivariate characteristics and their dependences are distinct among the regions of the island and thus need specific copulas to be modelled.

The copulas $C_{U,V}$ that best describe the observed dependence patterns between normalised values of previous NAOI, U , and of extreme rainfall, V are presented as contour lines in Figure 5. The normalisation of values was carried out to allow direct comparisons among the multivariate normal shapes of the rain gauge observations and bring out specific features, such as the dependence measure of tail dependence [48]. This allowed us to determine the level of association among extreme events in the lower and upper tails for previous NAOI and extreme rainfall, respectively. In this case, the previous NAOI lower tail corresponds to strongly negative previous NAOI values and the importance of this association lies in the fact that negative NAOI values have been connected to impacts on regional climate variability during winter (e.g., [55]).

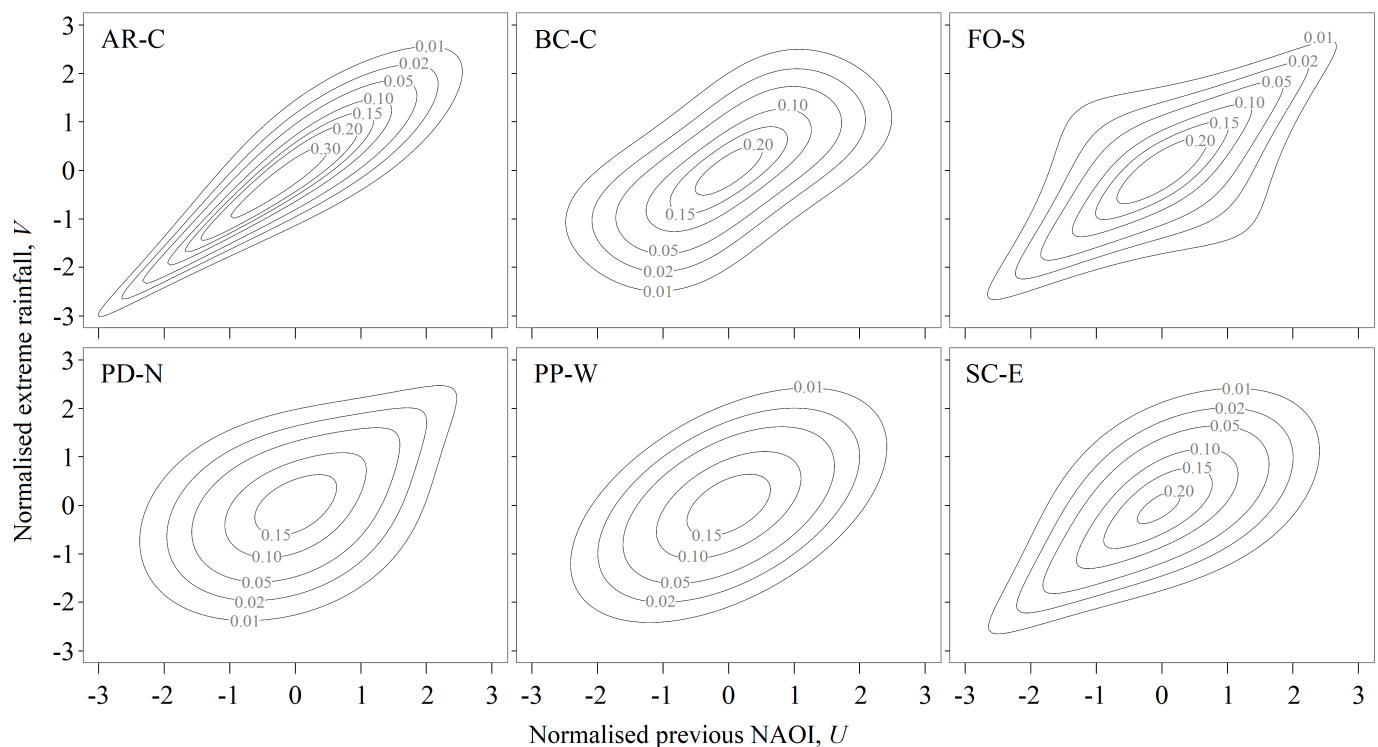


Figure 5. Normalised contour plots of the selected bivariate copulas—namely, Survival Gumbel (AR-C and SC-E), Frank (BC-C), Student’s t (FO-S), Gumbel (PD-N), and Gaussian (PP-W).

Table 4. Selected copula families, Kendall tau (τ), univariate distributions used for candidate of marginal distributions of *NI* and *RN*, and parameters of the models at each rain gauge. Par stands for the copula parameter, and Par1 and Par2 for the marginal distribution parameters.

Rain Gauge	Copula				Opposite Previous NAOI, <i>NI</i>				Extreme Rainfall, <i>RN</i>			
	Family	Par	τ	AIC	Univariate Dist.	Par1	Par2	AIC	Univariate Dist.	Par1	Par2	AIC
AR-C	Survival Gumbel	3.28	0.70	−66.61	log-normal	5.15	0.36	502.09	log-normal	5.09	0.17	429.61
BC-C	Frank	4.90	0.45	−18.91	log-normal	5.17	0.30	490.18	log-normal	5.05	0.21	445.14
FO-S	Student's <i>t</i>	0.63	0.44	−27.18	log-normal	5.07	0.42	509.67	log-normal	4.04	0.26	374.56
PD-N	Gumbel	1.38	0.28	−9.53	log-normal	5.10	0.39	506.36	log-normal	4.38	0.32	423.23
PP-W	Gaussian	0.50	0.33	−10.79	Weibull	2.32	196.04	522.39	log-normal	4.00	0.31	387.31
SC-E	Survival Gumbel	1.69	0.41	−16.43	log-normal	5.12	0.39	508.15	log-normal	4.02	0.22	357.72

Figure 5 shows that the Survival Gumbel copula (the rotated Gumbel copula) best-fitted the bivariate series at AR-C and SC-E rain gauges with a stronger dependency in the lower tail of previous NAOI and in the upper tail of extreme rainfall. On the other hand, the PD-N series presented a Gumbel copula with an inverted dependence structures. The copulas for FO-S and PP-W are of the same class, i.e., meta-elliptic copulas (Table 2), although with different dependence structure. The joint distribution at FO-S was modelled with a Student’s *t* copula by generating joint symmetric tail dependence, hence allowing an increased probability of joint extreme events. For the series at PP-W, the Gaussian copula was used by generating joint symmetric dependence, and, according to the copula’s characteristics, with no tail dependence, i.e., no joint extreme events. For BC-C, the goodness-of-fit test resulted in well-fitted Frank copula being symmetric and with more probability concentrated in the tails, but without lower or upper tail dependence. Rather than from just a linear correlation analysis, these results robustly evidence different dependence structures between previous NAOI and extreme rainfalls across the island.

4.4. Bivariate Return Periods of the Previous NAOI and Extreme Rainfall Events

The return periods $T_{NI \& RN}$, defined by Equation (8), of the 45 coupled events depending upon the modelled joint behaviour of the two random variables at each rain gauge are shown in Figure 6. Those with the highest return periods $T_{NI \& RN}$ are reported in Table 5. Since various combinations of previous NAOI and extreme rainfall can result in the same $T_{NI \& RN}$, the return periods are presented as contour lines in the figure. These lines are bounded by the axes and denote different patterns regarding the location of the rain gauge on the island. As an illustrative example, a combination of previous NAOI of -200 and a daily rainfall of 100 mm results in $T_{NI \& RN} \approx 3$ years at the central highlands (AR-C and BC-C), $T_{NI \& RN} \approx 90$ years on the southern lowland (FO-S), $T_{NI \& RN} \approx 9$ years on the northern slope (PD-N), $T_{NI \& RN} \approx 25$ years in the western area (PP-W), and $T_{NI \& RN} \approx 450$ years in the eastern region of the island (SC-E).

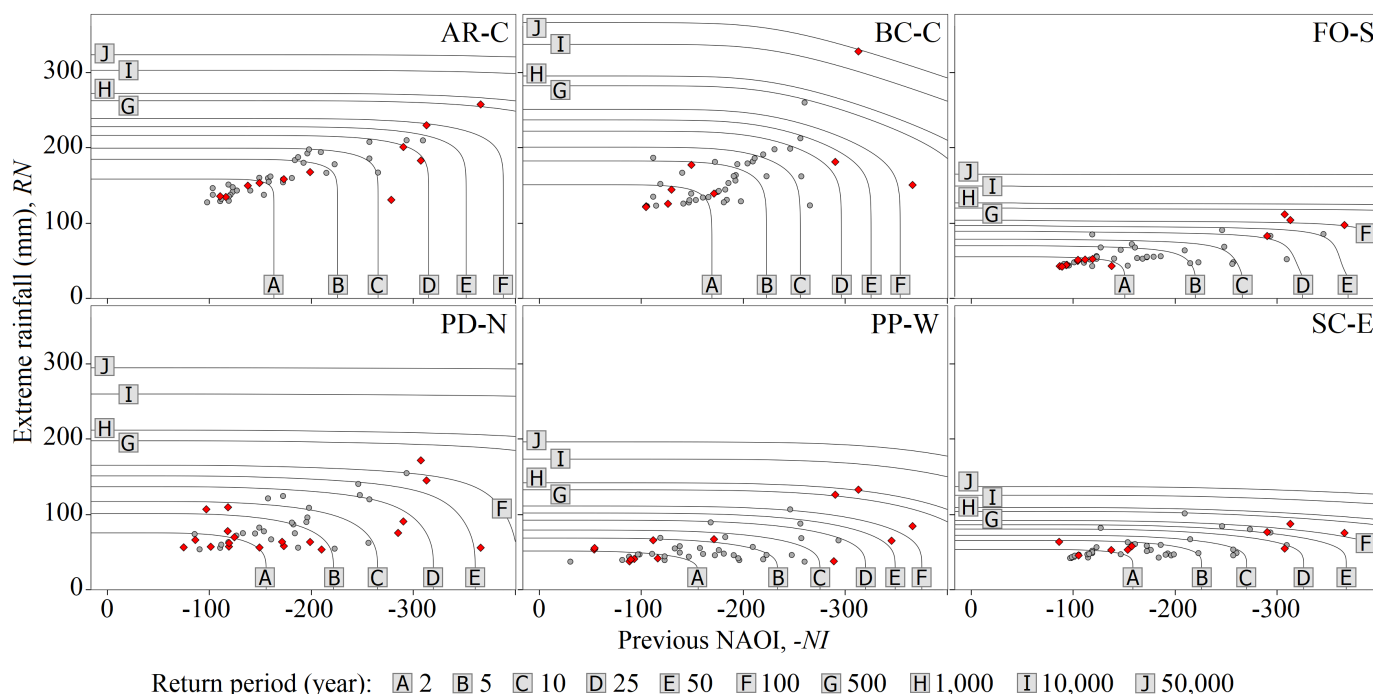


Figure 6. Contour lines of the joint return periods $T_{NI \& RN}$ of the 45 bivariate events in each rain gauge. The letters, from A to J, stand for the different return periods between 2 and 50,000 years. The events occurring from 1967/1968 to 1999/2000 are depicted by grey bullets, and those from 2000/2001 and 2016/2017 by red diamonds.

Figure 6 also presents the bivariate events, differentiating those from the initial 33-year sub-period, from December 1967 to February 2000, to the ones from the final 17-year sub-period, from December 2000 to February 2017. For the initial sub-period, this differentiation resulted in 33, 36, 32, 26, 32, and 35 extreme events for AR-C, BC-C, FO-S, PD-N, PP-W, and SC-E, respectively, and consequently, for the final sub-period, in 12, 9, 13, 19, 13, and 10 events. By dividing the number of events by the number of years of their respective sub-periods, interarrival times different to the one used to construct copulas were obtained. A comparison of the $E(L)$ between the two sub-periods revealed that for all the rain gauges, except for PD-N, $E(L)$ decreased, meaning less frequent extreme rainfall events in the last 17 years. However, the figure shows that the most extreme bivariate events with higher return periods, except for SC-E, always took place in the more recent sub-period.

Figure 7 depicts the conditional return periods, i.e., the return period of extreme rainfall, given that the previous NAOI is lower than a certain threshold. Note that the horizontal axes are always the same but the vertical axes are not. Moreover, some of the more exceptional bivariate events of Table 5 are not depicted in the figure due to the adopted vertical scales. For uniformity purposes, the reported events are those with the highest return periods associated with $T_{NI\ and\ RN}$, as previously mentioned. By way of example, for AR-C, regardless the return period approach, the most unusual event occurred in February 2010 with previous NAOI of -366.0 and extreme rainfall of 257.6 mm. The univariate analysis, based on the best-fitted marginal distribution and Equations (6) and (7), resulted in return periods of 491 and 2646 years, respectively. From the multivariate analysis, the joint return period (Equation (8)) is 4407 years, whereas the conditional one (Equation (9)) corresponds to 259,894 years.

Table 5. At each of the six rain gauges, dates and characteristics of the three bivariate observations (previous NAOI and extreme daily rainfalls) with the highest return periods $T_{NI\ and\ RN}$ and their corresponding univariate, bivariate, and conditional return periods rounded to the nearest integer in years.

Rain Gauge	Date $T_{NI\ \&\ RN}$	Previous NAOI, $-NI$	Extreme Rainfall (mm), RN	T_{NI} (year)	T_{RN} (year)	$T_{NI\ \&\ RN}$ (year)	$T_{RN NI\geq ni}$ (year)
AR-C	21/02/2010	-366.0	257.6	491	2646	4407	259,844
	26/01/2011	-313.0	230.0	180	422	674	14,560
	05/12/1991	-309.4	210.0	169	129	293	5922
BC-C	26/01/2011	-313.0	327.3	278	44,618	324,643	10,843,673
	15/12/1976	-260.2	259.6	82	1175	3010	29,683
	21/02/2010	-366.0	150.4	1009	15	1072	129,742
FO-S	02/02/2010	-307.4	111.0	143	1600	1991	34,109
	26/01/2011	-313.0	103.4	156	758	1011	18,887
	21/02/2010	-366.0	96.8	355	401	787	33,537
PD-N	02/02/2010	-307.4	172.1	152	1034	1525	27,882
	01/01/1969	-293.4	155.2	120	449	742	10,721
	26/01/2011	-313.0	145.5	167	279	598	12,010
PP-W	26/01/2011	-313.0	133.3	160	3794	7975	153,443
	27/02/2009	-290.3	126.6	100	2295	4157	49,821
	21/02/2010	-366.0	85.0	585	107	1348	94,663
SC-E	10/02/1969	-209.4	101.9	29	2642	3420	12,027
	26/01/2011	-313.0	88.0	151	432	1517	27,517
	21/02/2010	-366.0	76.0	364	104	1031	45,060

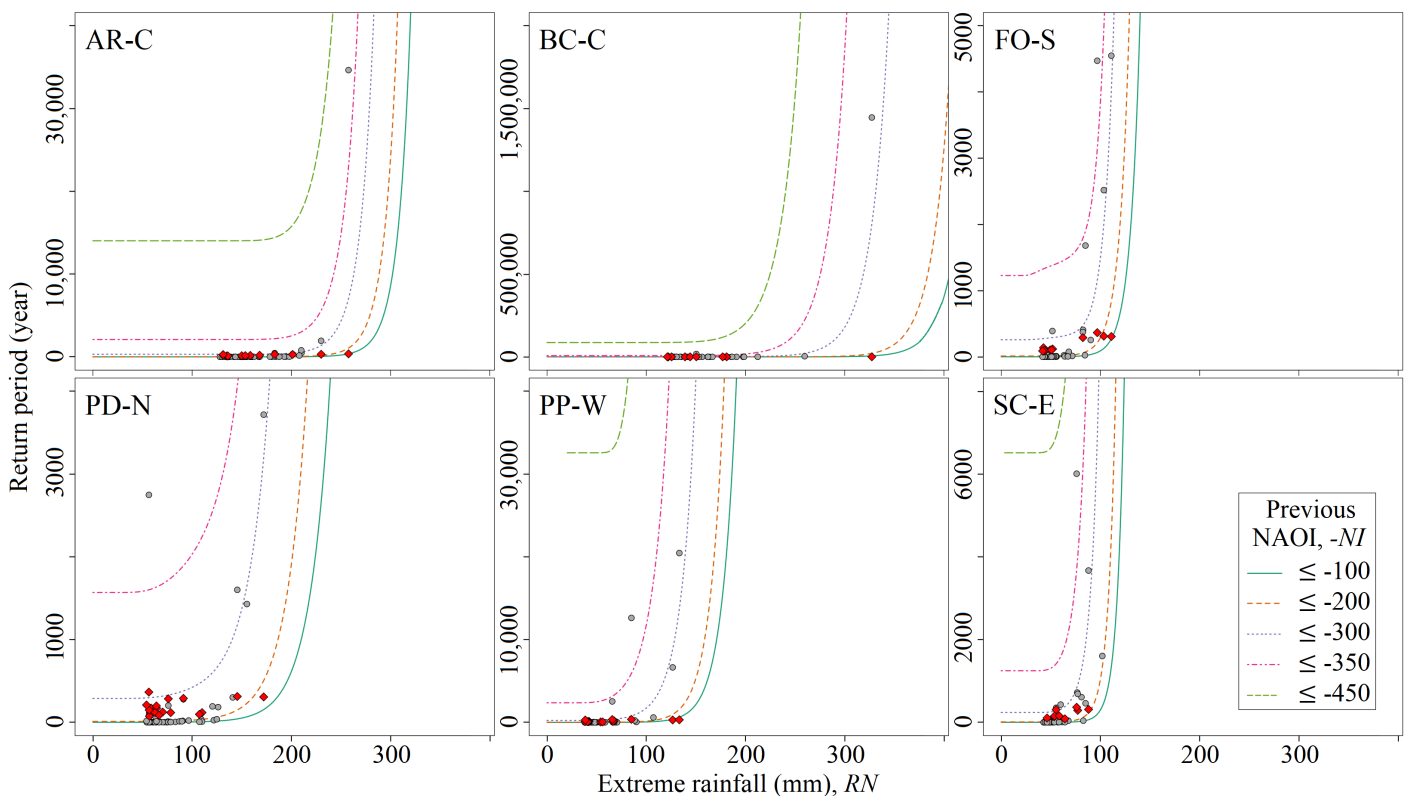


Figure 7. Conditional return periods $T_{RN|NI \geq ni}$ for different previous NAOI values. The bivariate observations from 1967/1968 to 1999/2000 are depicted by grey bullets, and from 2000/2001 and 2016/2017 by red diamonds.

In general terms, the achieved univariate and bivariate return periods from December 1967 to February 2017 show that the island has been characterised by numerous events with an unsteady chronological development, particularly with highly negative previous NAOI and more intense extreme rainfalls in earlier years. Based on the results shown in Figure 6 coupled with those reported in Table 5, from December 2010 to February 2011, the persistently negative phase of the NAO (in this case, previous NAOI) is according to the assumptions made for the bivariate problem in generating highly winter daily extreme rainfalls across Madeira. These observed extreme rainfall patterns can, however, be attributed—among other atmospheric processes—to the leading pattern of climate variability over the Northern Hemisphere, i.e., to the NAO variability.

5. Discussion and Conclusions

The influence of the NAO large-circulation pattern on 45 winter (DJF) extreme rainfalls (from December 1967 to February 2017) was examined at the daily scale for six rain gauges with apparently distinct microclimates and rainfall variability due to their locations on Madeira Island, i.e., in the northern, southern, eastern and western coastal zones, and in the central highlands. This influence was addressed by using an index, selected among others [56], capturing representative daily spatiotemporal-dependent features associated with the pattern in SLP over the North Atlantic sector or with the NAO pattern, i.e., daily NAOI, coupled with daily rainfall records. Accordingly, this research work delineates a systematic analysis of the jointly modelling of NAOI for the same day or prior to the occurrence of extreme rainfall events via bivariate copulas. To do so, in the initial stage of this research work, the cause–effect degree between (i) non-smoothed and smoothed NAOI values and (ii) extreme daily rainfall events was measured. This process enabled the assembly of the final dataset representing the core for copula modelling describing the dependence characteristics of the analysed bivariate problem. The copula modelling also ascertained long-distance relationships between random events of previous NAOI and

extreme rainfall on the island, i.e., teleconnections, specifically used for the calculation of bivariate return periods, and thus making a climate variability assessment.

5.1. Negative NAO Persistence and Climate Variability

Despite that the shifts in the NAO do not necessarily create simultaneous, symmetrical rainfall imbalances or anomalies, this research work ascertained an atmospheric configuration resulting in strongly negative Pearson correlation (r) for the bivariate coupled events for the Areeiro rain gauge. Note that all the previous NAOI values associated with the 45 extreme rainfalls at each rain gauge were negative (plotted in Figure 6) and part of negative NAO phases, i.e., of weaker than usual differences in pressure [12]. This reinforces the hypothesis that during winter—the time when the NAO pattern is very strong and broadly extended [56]—the impacts on climate variability are produced mainly by persistent figures of negative NAO.

The correlation (r) between previous NAOI and extreme rainfall is consistently below than -0.50 , except for the northern slope, namely, -0.84 (AR-C), -0.58 (BC-C), -0.69 (FO-S), -0.48 (PD-N), -0.52 (PP-W), and -0.52 (SC-E). Although the correlation always portrays a symmetrical association, it differs among rain gauges, suggesting different extremal rainfall behaviours. Additionally, a comparison was carried out between the ratios of long-term rainfall average of the 4,500 daily rainfalls (11.36, 11.68, 3.04, 4.67, 3.44, and 3.21 mm, respectively, for AR-C, BC-C, FO-S, PD-N, PP-W, and SC-E) and their respective mean extreme values (reported in Table 3). Accordingly, this revealed that greater ratios characterised the coastal zones, highlighting their greater vulnerability to extreme rainfall events from 1967/1968 through 2016/2017 than the central highlands, which, however, experienced high heavy rainfall. This indicated—and confirmed later with the copula modelling—that the studied bivariate phenomenon or climate variability in the assembled dataset has marked interisland variation.

5.2. Copula-Based Modelling of NAO Teleconnection in Extreme Rainfall

The preliminary results indicated that the interannual variability of extreme winter rainfall—which is often high on small islands as on Madeira [32]—was largely modulated by the NAO mode. Such a noticeable influence on extreme events required a multidimensional analysis of the random variables. The modelling of dependence structure conventionally assumes, directly or indirectly, linear correlation given through the Pearson correlation coefficient, r [57]. However, as mentioned, the studied NAO phenomena are particularly complex and are made up of a combination of different stochastic processes. Thus, a bivariate approach [44] using copulas was used in each of the rain gauges to skirt these constraints by allowing the independent modelling of univariate marginals and of non-linear dependence structures between two vectors. Additionally, the copulas were adopted due to their flexibility and the various types of dependence that they allow for, and as they do not depend on the marginal distributions F_X and F_Y [58,59]. To measure the association among the random variables, the Kendall's τ correlation coefficient was used instead to overcome the shortcoming of the r coefficient. The τ coefficient varied from strong (at AR-C) to moderate for the bivariate observations (see Table 3). The difference in τ correlation may be due to the model establishment (based on a single rain gauge, AR-C) but also to internal climate variability or other sources of rainfall variability across the island. In any case, to build a copula, the degree of association in some way must be assessed [60] but keeping in mind that the resulting copulas are conditional upon to the array used. Note that negative correlations affect the types of copulas that can be employed in this study, as some copulas exist only in the positive dependence space. To circumvent this hurdle and not double the number of copulas in the analysis (e.g., by including rotated versions of Archimedean copula families), the copulas were modelled with opposite previous NAOI series (NI), instead of the negative series.

5.3. Climate Variability Assessment Based on the Bivariate Return Periods

The return periods achieved using copulas highlight the importance of modelling the joint behaviour of previous NAOI and extreme rainfall. The bivariate modelling may simplify the calculations, and unveil the mechanism of structure-dependent behaviour of the phenomena of interest. From the analysed joint events, well-defined marginal probability distributions were established, which, in turn, allowed calculating the joint probability and thus estimating contour lines of the return period. This adopted bivariate approach contrasts with those traditionally implemented for assessing bivariate return periods of specific extreme hydrological events. As an example, Kim et al. [61] assessed the hydrological risk based on univariate and multivariate density functions, although the authors state that the joint density is not mathematically manageable. Additionally, a comparison of the joint and conditional return periods to those separately calculated (Table 5) shows that univariate approaches may underestimate the risk related to specific events. Therefore, the multivariate analysis seems to have advantages over univariate applications by defining a more complex dependence structure closer to reality. Nevertheless, it is acknowledged that future work should quantitatively investigate the integration of another large-scale circulation pattern—such as El Niño Southern Oscillation (ENSO) [62]—in the climate variability assessment for a more dynamical analysis (e.g., [57,63]), and for addressing the remarkable transition toward a warmer winter climate regime, i.e., sustained higher GTS [7,64].

Detecting variations in extreme rainfall series and the large-scale modes that generate those variations are crucial to identify climate variability, which is generally characterised by anomalous extreme events. Such anomalies clearly outnumber the bivariate long-term average, as demonstrated in the current analysis. Figure 6 (and also Figure 7, although with truncated vertical axes) covers most of the results obtained with coherent responses and relationships at different degrees between extreme rainfall patterns with respect to the previous NAOI. These also show that as the previous NAOI gets more negative, the return period curves are more dependent on the development of this index. That is, for a given extreme rainfall, its return period is constant or almost constant for the higher NAOI values. As the previous NAOI values become more negative, the return period can increase substantially as a result of the exceptionality of the bivariate event. This strongly suggests that the previous NAOI (i) is the main trigger of the winter (DJF) extreme daily rainfalls, and that it (ii) contains information regarding the antecedent atmospheric conditions. These results clearly show that the identified DJF extreme rainfalls can be associated with changes in the previous NAOI signal—further reading on the dynamic mechanisms of extreme rainfall and the negative phase of NAO in Madeira can be found in [18]. Moreover, the same figures depict the noticeable increase in intensity in the joint behaviour of previous NAOI (highly negative) and extreme rainfall in earlier years. These results are corroborative evidence of increased climate variability in Madeira accompanied by a remarkable increase in variability in the NAO, specifically toward the persistence of a negative winter NAO, from ca. early 2000s onwards—as identified by Taws et al. [64], Hanna et al. [65], Hanna and Cropper [17].

5.4. Challenges and Advances Related to Extreme Rainfall Analyses

The remarkable identified bivariate events of winters of 2009/2010 and 2010/2011 (some of the most intense events ever recorded) further emphasise the challenges for climate variability assessment for the small island of Madeira. Note that small island environments are highly vulnerable to natural disasters such as cyclones and storm surges. They are also susceptible to flash floods, landslides and debris flows as a result of extreme rainfall [32]. It is therefore essential to study variability of extreme rainfall at shorter time scales along with atmospheric observations from a multivariate perspective. This in turn may help to understand the atmospheric physics and the mechanisms that can shift a heavy rain event into one producing floods on the island. Even though the teleconnection based on copulas is not well-established for all the analysed rain gauges, it is still essential for

planning water-related activities considering the vulnerability of the island to large-scale climatic variations.

Author Contributions: Conceptualisation, L.A.E.; methodology, L.A.E. and J.D.P.F.; software, J.D.P.F. and L.A.E.; validation, M.M.P. and J.D.P.F.; formal analysis, L.A.E. and J.D.P.F.; investigation, L.A.E.; resources, L.A.E.; data curation, L.A.E.; writing—original draft preparation, L.A.E.; writing—review and editing, M.Z. and M.M.P.; visualisation, L.A.E. and J.D.P.F.; supervision, M.M.P. All authors have read and agreed to the published version of the manuscript.

Funding: The work of the first author is funded by the Portuguese Foundation for Science and Technology (FCT), grant No. PD/BD/128509/2017; regarding the second and fourth authors also by FCT, within the project Scientific Cooperation Agreement between Portugal and Slovakia–2019/2020, SK-PT-18-0008; and for the third author by the Coordenação de Aperfeiçoamento de Pessoal de Nível Superior, Brasil (CAPES), Finance Code 001.

Data Availability Statement: The data that support the findings of this study are available on request from the corresponding author, L.A.E.

Acknowledgments: The authors thank IPMA for providing most of the daily and sub-daily rainfall data used in this analysis.

Conflicts of Interest: The authors declare no conflict of interest.

References

- Folland, C.K.; Karl, T.R.; Jim Salinger, M. Observed climate variability and change. *Weather* **2002**, *57*, 269–278. [[CrossRef](#)]
- Cuspilici, A.; Monforte, P.; Ragusa, M. Study of Saharan dust influence on PM10 measures in Sicily from 2013 to 2015. *Ecol. Indic.* **2017**, *76*, 297–303. [[CrossRef](#)]
- Yu, B.; Neil, D. Long-term variations in regional rainfall in the south-west of Western Australia and the difference between average and high intensity rainfalls. *Int. J. Climatol.* **1993**, *13*, 77–88. [[CrossRef](#)]
- Iliopoulou, T.; Koutsoyiannis, D. Projecting the future of rainfall extremes: Better classic than trendy. *J. Hydrol.* **2020**, *588*, 125005. [[CrossRef](#)]
- Haylock, M.; Goodess, C. Interannual variability of European extreme winter rainfall and links with mean large-scale circulation. *Int. J. Climatol. A J. R. Meteorol. Soc.* **2004**, *24*, 759–776. [[CrossRef](#)]
- Scaife, A.A.; Folland, C.K.; Alexander, L.V.; Moberg, A.; Knight, J.R. European climate extremes and the North Atlantic Oscillation. *J. Clim.* **2008**, *21*, 72–83. [[CrossRef](#)]
- Kharin, V.V.; Zwiers, F.; Zhang, X.; Wehner, M. Changes in temperature and precipitation extremes in the CMIP5 ensemble. *Clim. Chang.* **2013**, *119*, 345–357. [[CrossRef](#)]
- Sillmann, J.; Kharin, V.; Zhang, X.; Zwiers, F.; Bronaugh, D. Climate extremes indices in the CMIP5 multimodel ensemble: Part 1. Model evaluation in the present climate. *J. Geophys. Res. Atmos.* **2013**, *118*, 1716–1733. [[CrossRef](#)]
- Sillmann, J.; Kharin, V.V.; Zwiers, F.; Zhang, X.; Bronaugh, D. Climate extremes indices in the CMIP5 multimodel ensemble: Part 2. Future climate projections. *J. Geophys. Res. Atmos.* **2013**, *118*, 2473–2493. [[CrossRef](#)]
- Pendergrass, A.G.; Hartmann, D.L. The atmospheric energy constraint on global-mean precipitation change. *J. Clim.* **2014**, *27*, 757–768. [[CrossRef](#)]
- Visbeck, M.H.; Hurrell, J.W.; Polvani, L.; Cullen, H.M. The North Atlantic Oscillation: Past, present, and future. *Proc. Natl. Acad. Sci. USA* **2001**, *98*, 12876–12877. [[CrossRef](#)] [[PubMed](#)]
- Ferrari, E.; Caloiero, T.; Coscarelli, R. Influence of the North Atlantic Oscillation on winter rainfall in Calabria (southern Italy). *Theor. Appl. Climatol.* **2013**, *114*, 479–494. [[CrossRef](#)]
- Trigo, R.M.; Zêzere, J.L.; Rodrigues, M.L.; Trigo, I.F. The influence of the North Atlantic Oscillation on rainfall triggering of landslides near Lisbon. *Nat. Hazards* **2005**, *36*, 331–354. [[CrossRef](#)]
- Charlery, J.; Nurse, L.; Whitehall, K. Exploring the relationship between the North Atlantic oscillation and rainfall patterns in Barbados. *Int. J. Climatol. A J. R. Meteorol. Soc.* **2006**, *26*, 819–827. [[CrossRef](#)]
- Tabari, H.; Willems, P. Lagged influence of Atlantic and Pacific climate patterns on European extreme precipitation. *Sci. Rep.* **2018**, *8*, 1–10. [[CrossRef](#)] [[PubMed](#)]
- López-Moreno, J.I.; Vicente-Serrano, S.M. Positive and negative phases of the wintertime North Atlantic Oscillation and drought occurrence over Europe: A multitemporal-scale approach. *J. Clim.* **2008**, *21*, 1220–1243. [[CrossRef](#)]
- Hanna, E.; Cropper, T.E. North Atlantic Oscillation. In *Oxford Research Encyclopedia of Climate Science*; Oxford Research Encyclopedias: Oxford, UK, 2017. [[CrossRef](#)]
- Espinosa, L.A.; Portela, M.M.; Rodrigues, R. Significant Extremal Dependence of a Daily North Atlantic Oscillation Index (NAOI) and Weighted Regionalised Rainfall in a Small Island Using the Extremogram. *Water* **2020**, *12*, 2989. [[CrossRef](#)]
- Cropper, T. The weather and climate of Macaronesia: Past, present and future. *Weather* **2013**, *68*, 300–307. [[CrossRef](#)]
- Walker, G.; Bliss, W. World Weather V. Memories of the Royal Meteorological. *Society* **1932**, *44*, 53–84.

21. Wallace, J.M.; Gutzler, D.S. Teleconnections in the geopotential height field during the Northern Hemisphere winter. *Mon. Weather Rev.* **1981**, *109*, 784–812. [[CrossRef](#)]
22. Fragoso, M.; Trigo, R.; Pinto, J.; Lopes, S.; Lopes, A.; Ulbrich, S.; Magro, C. The 20 February 2010 Madeira flash-floods: Synoptic analysis and extreme rainfall assessment. *Nat. Hazards Earth Syst. Sci.* **2012**, *12*, 715–730. [[CrossRef](#)]
23. Jung, T.; Vitart, F.; Ferranti, L.; Morcrette, J.J. Origin and predictability of the extreme negative NAO winter of 2009/10. *Geophys. Res. Lett.* **2011**, *38*. [[CrossRef](#)]
24. Wilby, R.; O'hare, G.; Barnsley, N. The North Atlantic Oscillation and British Isles climate variability, 1865–1996. *Weather* **1997**, *52*, 266–276. [[CrossRef](#)]
25. Trambly, Y.; El Adlouni, S.; Servat, E. Trends and variability in extreme precipitation indices over Maghreb countries. *Nat. Hazards Earth Syst. Sci.* **2013**, *13*, 3235–3248. [[CrossRef](#)]
26. Wang, C.; Deser, C.; Yu, J.Y.; DiNezio, P.; Clement, A. El Niño and southern oscillation (ENSO): A review. In *Coral Reefs of the Eastern Tropical Pacific*; Springer Nature: Cham, Switzerland, 2017; pp. 85–106.
27. Queralt, S.; Hernández, E.; Barriopedro, D.; Gallego, D.; Ribera, P.; Casanova, C. North Atlantic Oscillation influence and weather types associated with winter total and extreme precipitation events in Spain. *Atmos. Res.* **2009**, *94*, 675–683. [[CrossRef](#)]
28. Embrechts, P.; Lindskog, F.; McNeil, A. *Modelling Dependence with Copulas*; Rapport Technique; Département de Mathématiques, Institut Fédéral de Technologie de Zurich: Zurich, Switzerland, 2001; Volume 14.
29. Wong, G.; Lambert, M.F.; Metcalfe, A.V. Trivariate copulas for characterisation of droughts. *Anziam J.* **2007**, *49*, C306–C323. [[CrossRef](#)]
30. André, L.; de Zea Bermudez, P. Modelling dependence between observed and simulated wind speed data using copulas. *Stoch. Environ. Res. Risk Assess.* **2020**, *34*, 1725–1753. [[CrossRef](#)]
31. Gouveia-Reis, D.; Lopes, L.G.; Mendonça, S. A dependence modelling study of extreme rainfall in Madeira Island. *Phys. Chem. Earth, Parts A/B/C* **2016**, *94*, 85–93. [[CrossRef](#)]
32. Falkland, A.; Custodio, E. *Hydrology and Water Resources of Small Islands: A Practical Guide*; UNESCO: London, UK, 1991; Volume 49.
33. Prada, S.; da Silva, M. Fog precipitation on the Island of Madeira (Portugal). *Environ. Geol.* **2001**, *41*, 384–389. [[CrossRef](#)]
34. Santos, F.; Valente, M.; Miranda, P.; Aguiar, A.; Azevedo, E.; Tomé, A.; Coelho, F. Climate change scenarios in the Azores and Madeira islands. *World Resour. Rev.* **2004**, *16*, 473–491.
35. Chazarra, A.; Banceló, A.; Pires, V.; Cunha, S.; Silva, A.; Marques, J.; Carvalho, F.; Mendes, M.; Neto, J.; Mendes, L. Climate Atlas of the Archipelagos of the Canary Islands. *Madeira and the Azores*; Department of Meteorology and Climatology of the Institute of Meteorology: Lisbon, Portugal, 2011.
36. Black, D.E.; Peterson, L.C.; Overpeck, J.T.; Kaplan, A.; Evans, M.N.; Kashgarian, M. Eight centuries of North Atlantic Ocean atmosphere variability. *Science* **1999**, *286*, 1709–1713. [[CrossRef](#)] [[PubMed](#)]
37. Espinosa, L.A.; Portela, M.M. Rainfall trends over a small island teleconnected to the North Atlantic oscillation—the case of Madeira Island, Portugal. *Water Resour. Manag.* **2020**, *34*, 4449–4467. [[CrossRef](#)]
38. Klein Tank, A.; Peterson, T.; Quadir, D.; Dorji, S.; Zou, X.; Tang, H.; Santhosh, K.; Joshi, U.; Jaswal, A.; Kolli, R.; et al. Changes in daily temperature and precipitation extremes in central and south Asia. *J. Geophys. Res. Atmos.* **2006**, *111*, 1–8. [[CrossRef](#)]
39. Hair, J.; Black, W.; Babin, B.; Anderson, R.; Tatham, R. *Multivariate Data Analysis*; Prentice Hall: Hoboken, NJ, USA, 1998; Volume 5, pp. 207–219.
40. Golestan, S.; Ramezani, M.; Guerrero, J.M.; Freijedo, F.D.; Monfared, M. Moving average filter based phase-locked loops: Performance analysis and design guidelines. *IEEE Trans. Power Electron.* **2013**, *29*, 2750–2763. [[CrossRef](#)]
41. WMO (World Meteorological Organization). *Guide to Hydrological Practices, Volume II Management of Water Resources and Application of Hydrological Practices*; WMO (World Meteorological Organization): Geneva, Switzerland, 2009.
42. Espinosa, L.A.; Portela, M.M.; Rodrigues, R. Rainfall trends over a North Atlantic small island in the period 1937/1938–2016/2017 and an early climate teleconnection. *Theoretical Appl. Climatol.* **2021**, 1–23. [[CrossRef](#)]
43. NOAA. Daily Climate Timeseries: NAO: NOAA PSL. 2020. Available online: <https://psl.noaa.gov/data/timeseries/daily/NAO/> (accessed on 2 January 2021).
44. Sklar, M. Fonctions de repartition an dimensions et leurs marges. *Publ. Inst. Statist. Univ. Paris* **1959**, *8*, 229–231.
45. Schweizer, B.; Sklar, A. *Probabilistic Metric Spaces*; Courier Corporation: Chelmsford, MA, USA, 2011.
46. Nelsen, R.B. Methods of constructing copulas. In *An Introduction to Copulas*; Springer: Berlin/Heidelberg, Germany, 2006; pp. 51–108.
47. Joe, H. *Multivariate Models and Multivariate Dependence Concepts*; CRC Press: Boca Raton, FL, USA, 1997.
48. Brechmann, E.; Schepsmeier, U. Cdvine: Modeling dependence with c-and d-vine copulas in R. *J. Stat. Softw.* **2013**, *52*, 1–27. [[CrossRef](#)]
49. Shiau, J.T.; Shen, H.W. Recurrence analysis of hydrologic droughts of differing severity. *J. Water Resour. Plan. Manag.* **2001**, *127*, 30–40. [[CrossRef](#)]
50. Shiau, J.T. Return period of bivariate distributed extreme hydrological events. *Stoch. Environ. Res. Risk Assess.* **2003**, *17*, 42–57. [[CrossRef](#)]
51. Kwon, H.H.; Lall, U. A copula-based nonstationary frequency analysis for the 2012–2015 drought in California. *Water Resour. Res.* **2016**, *52*, 5662–5675. [[CrossRef](#)]

52. Shiau, J.T. Fitting drought duration and severity with two-dimensional copulas. *Water Resour. Manag.* **2006**, *20*, 795–815. [[CrossRef](#)]
53. Salazar, Y. General multivariate dependence using associated copulas. *Stat. J.* **2011**, *14*, 1–28. [[CrossRef](#)]
54. Venter, G. Tails of Copulas. *Proc. Casualty Actuar. Soc.* **2002**, *89*, 70–75.
55. Huang, J.; Ji, M.; Higuchi, K.; Shabbar, A. Temporal structures of the North Atlantic Oscillation and its impact on the regional climate variability. *Adv. Atmos. Sci.* **2006**, *23*, 23–32. [[CrossRef](#)]
56. Jianping, L.; Wang, J.X. A new North Atlantic Oscillation index and its variability. *Adv. Atmos. Sci.* **2003**, *20*, 661–676. [[CrossRef](#)]
57. Khedun, C.P.; Mishra, A.K.; Singh, V.P.; Giardino, J.R. A copula-based precipitation forecasting model: Investigating the interdecadal modulation of ENSO's impacts on monthly precipitation. *Water Resour. Res.* **2014**, *50*, 580–600. [[CrossRef](#)]
58. Embrechts, P.; Mcneil, E.; Straumann, D. Correlation: Pitfalls and alternatives. In *Risk Magazine*; Citeseer: Princeton, NJ, USA, 1999.
59. Abadi, M.S.E. Analysis of New Techniques for Risk Aggregation and Dependence Modelling. Ph.D. Thesis, Instituto Superior de Economia e Gestão, Lisbon, Portugal, 2015.
60. Clemen, R.T.; Reilly, T. Correlations and copulas for decision and risk analysis. *Manag. Sci.* **1999**, *45*, 208–224. [[CrossRef](#)]
61. Kim, T.W.; Valdés, J.B.; Yoo, C. Nonparametric approach for estimating return periods of droughts in arid regions. *J. Hydrol. Eng.* **2003**, *8*, 237–246. [[CrossRef](#)]
62. Sun, X.; Renard, B.; Thyer, M.; Westra, S.; Lang, M. A global analysis of the asymmetric effect of ENSO on extreme precipitation. *J. Hydrol.* **2015**, *530*, 51–65. [[CrossRef](#)]
63. Hui-Mean, F.; Yusof, F.; Yusop, Z.; Suhaila, J. Trivariate copula in drought analysis: A case study in peninsular Malaysia. *Theor. Appl. Climatol.* **2019**, *138*, 657–671. [[CrossRef](#)]
64. Taws, S.L.; Marsh, R.; Wells, N.C.; Hirschi, J. Re-emerging ocean temperature anomalies in late-2010 associated with a repeat negative NAO. *Geophys. Res. Lett.* **2011**, *38*. [[CrossRef](#)]
65. Hanna, E.; Cropper, T.E.; Jones, P.D.; Scaife, A.A.; Allan, R. Recent seasonal asymmetric changes in the NAO (a marked summer decline and increased winter variability) and associated changes in the AO and Greenland Blocking Index. *Int. J. Climatol.* **2015**, *35*, 2540–2554. [[CrossRef](#)]